# Supporting Information

# Elevated interstitial flow in the cerebrospinal fluid microenvironment accelerates glioblastoma cell migration on microfluidic chip

Wanting Hu [a], Hua Sun [a], Huibo Qi [a], Linkai Jiang [b], Kaining Zhang [c], Xiaomeng Jia [a], Yu Wang [a], Yu Xiang [c], and Qionglin Liang *[a]

a MOE Key Laboratory of Bioorganic Phosphorus Chemistry & Chemical Biology, Department of Chemistry, Laboratory of Flexible Electronics Technology, Center for Synthetic and Systems Biology, Tsinghua University, Beijing 100084, P.R. China

b Department of Mechanical Engineering, Tsinghua University, Beijing 100084, P.R. China

c Department of Chemistry, Beijing Key Laboratory for Microanalytical Methods and Instrumentation, Key Laboratory of Bioorganic Phosphorus Chemistry and Chemical Biology (Ministry of Education), Tsinghua University, Beijing, 100084, P.R. China

* Corresponding author at Department of Chemistry, Tsinghua University, Beijing 100084, P.R. China.

E-mail: liangql@tsinghua.edu.cn

# Contents

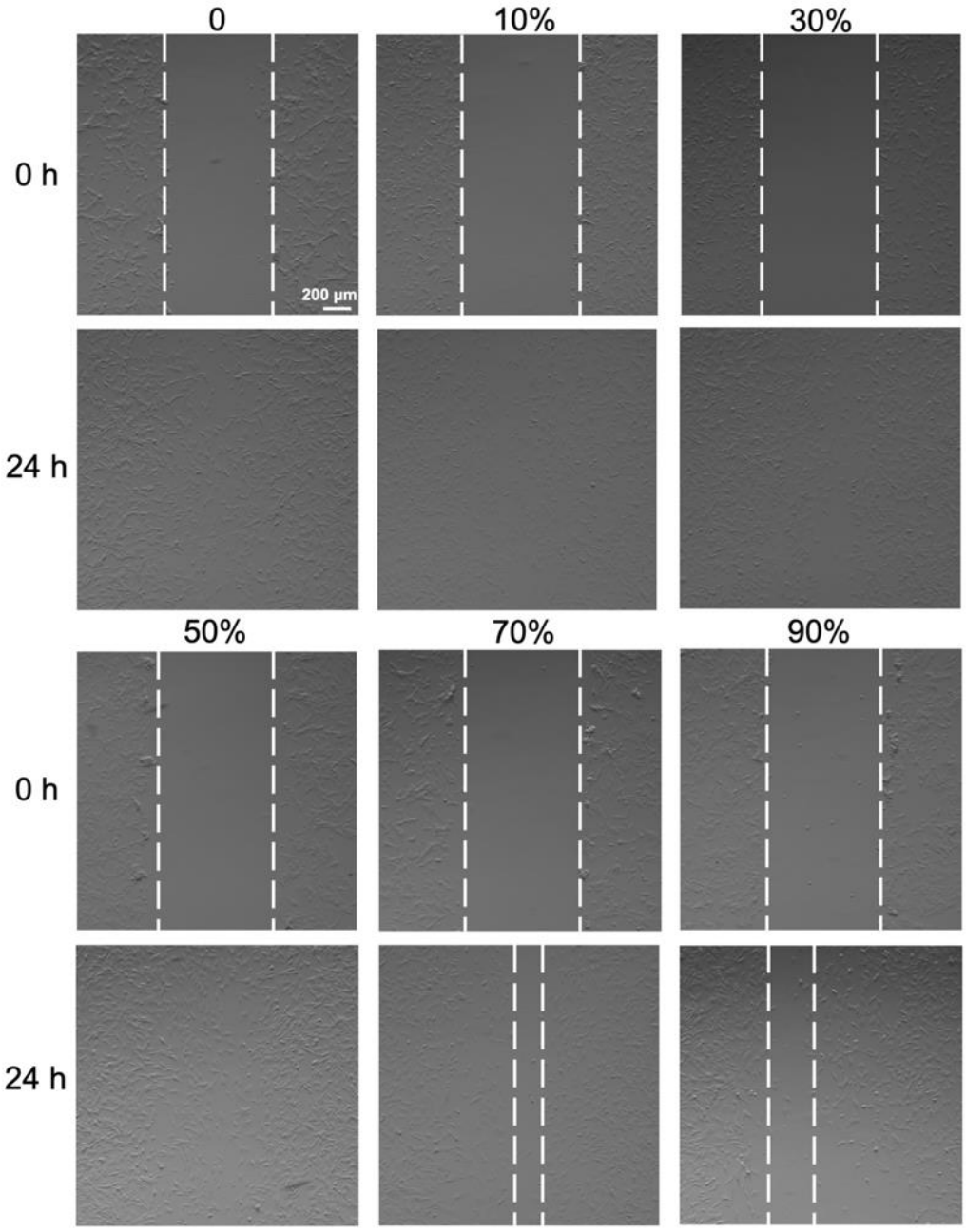


**Fig. S1** Representative images of ACSF mixture and 100% DMEM solution (control) from a wound healing assay.

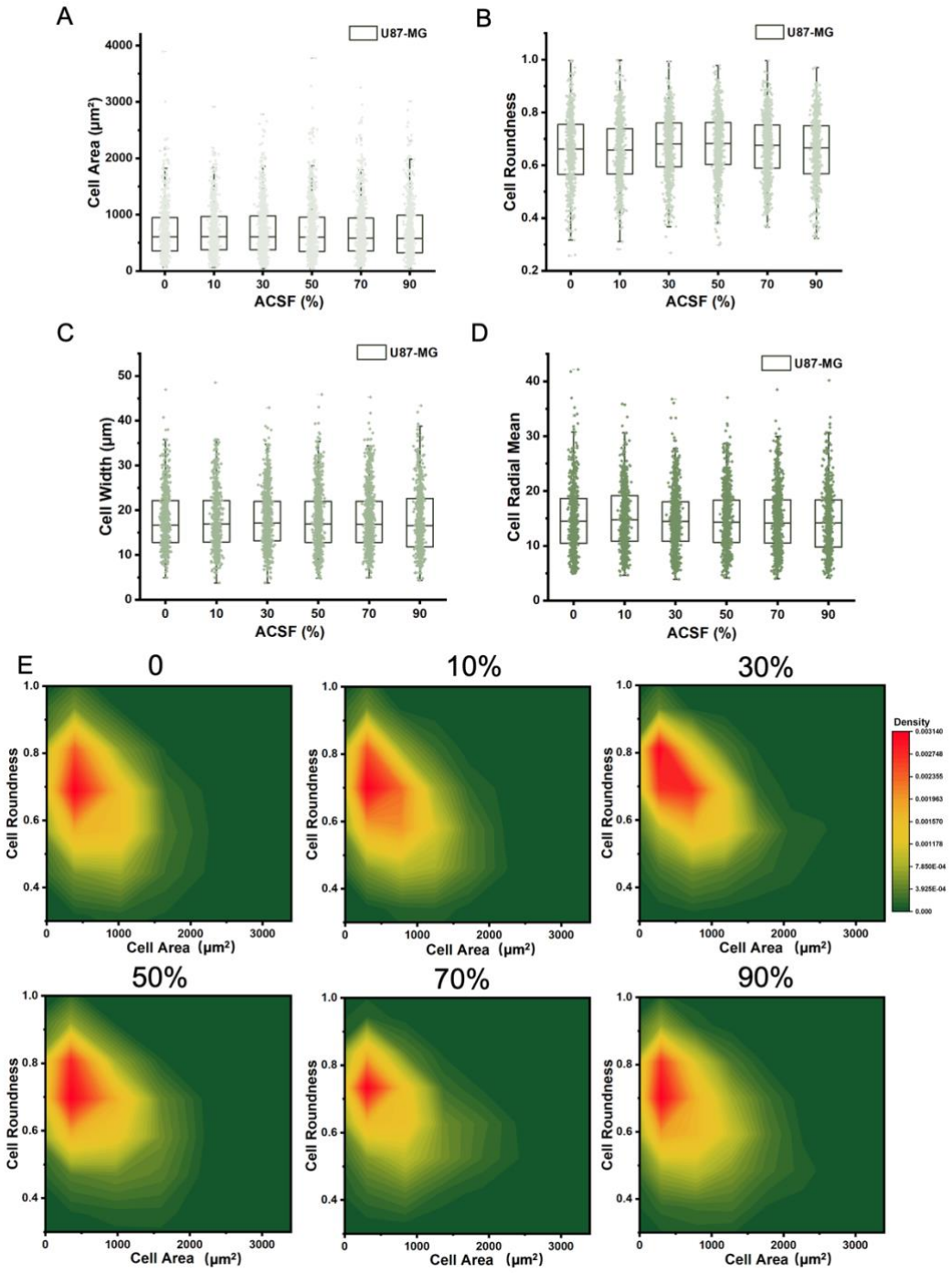


**Fig. S2** Effects of different concentrations of ACSF and 100% DMEM solution on morphology of U87-MG cell. (A-D) Effects of different concentrations of ACSF and 100% DMEM solution on morphologies of single U87-MG cell, including (A) cell area, (B) cell roundness, (C) cell width, (D) and cell radial mean. (E) Density distribution of cell area and cell roundness for different concentrations of ACSF and 100% DMEM solution.

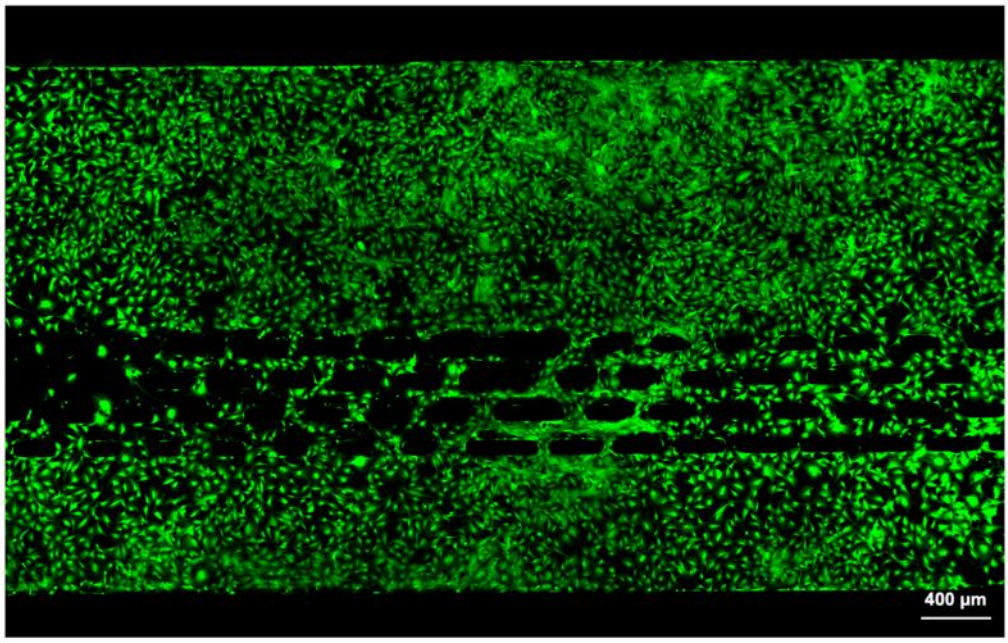


**Fig. S3** Representative fluorescent images of U87-MG cells cultured on the microfluidic chip for 10 days, and cells maintained their healthy morphology and proliferate. Scale bars, 400 μm.

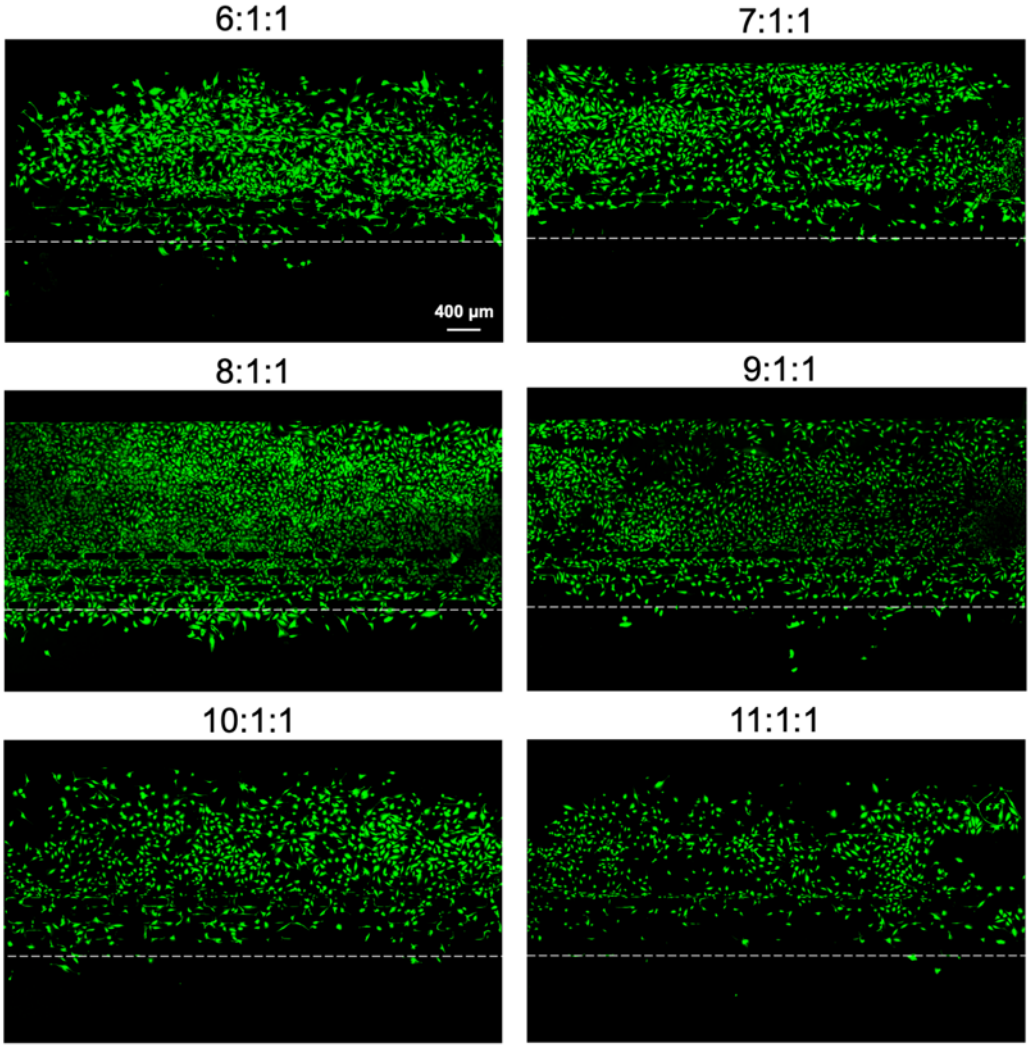


**Fig. S4** The optimal conditions for U87-MG cell culture were obtained by optimising the ratio of collagen:10× MEM:NaOH in the presence of interstitial flow, and the optimal cell culture conditions were collagen:10× MEM:NaOH = 8:1:1. Scale bars, 400 μm.

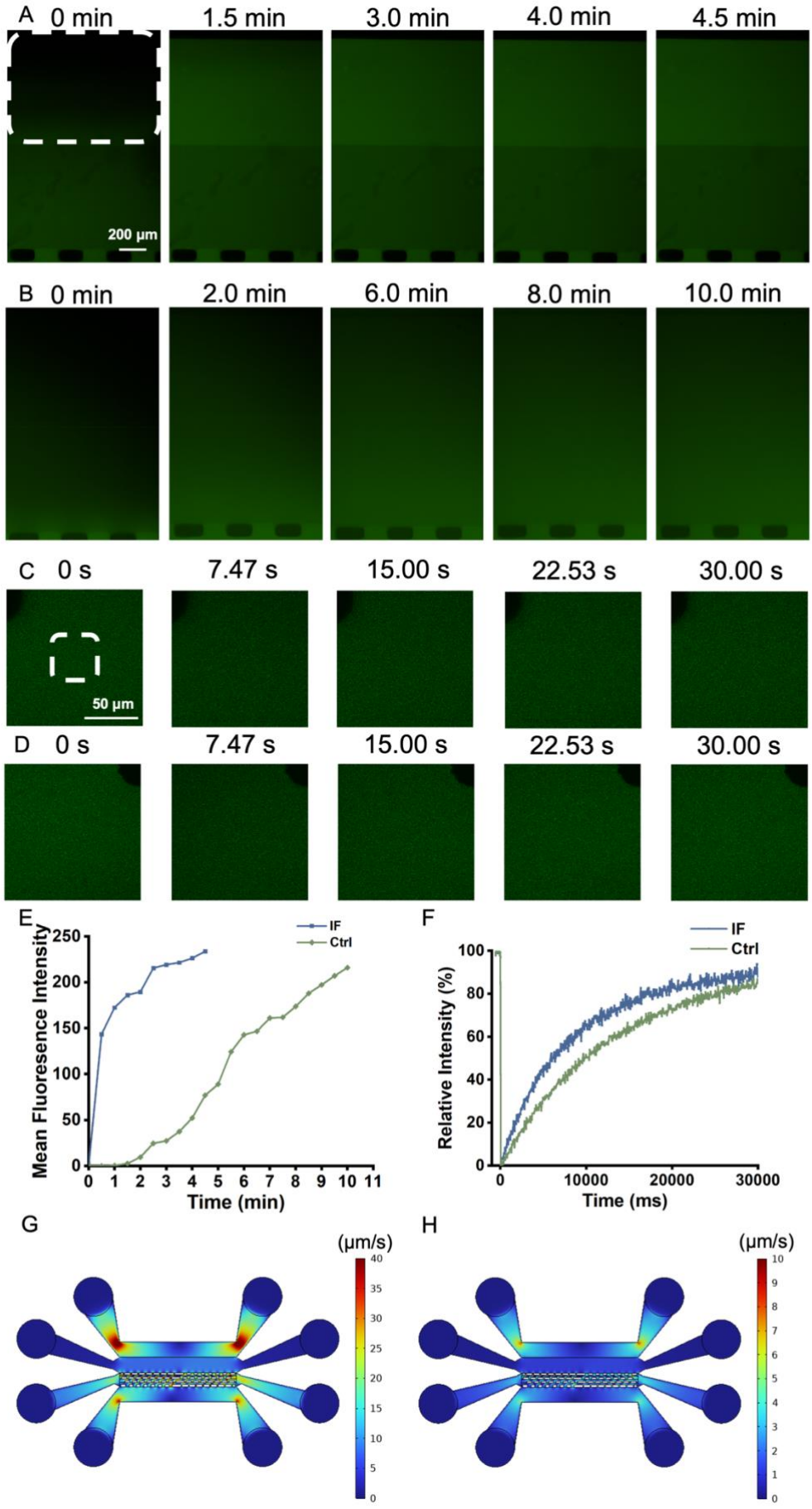
A
0 min
1.5 min
3.0 min
4.0 min
4.5 min
200 μm
B
0 min
2.0 min
6.0 min
8.0 min
10.0 min
C
0 s
7.47 s
15.00 s
22.53 s
30.00 s
50 μm
D
0 s
7.47 s
15.00 s
22.53 s
30.00 s
E
Mean Fluorescence Intensity
IF
Ctrl
Time (min)
F
Relative Intensity (%)
IF
Ctrl
Time (ms)
G
(μm/s)
H
(μm/s)

**Fig. S5** Characterization of interstitial flow (IF). (A-B) Representative fluorescence images of diffusion of sodium fluorescein solution in collagen-containing microfluidic chips in the (A) presence or (B) absence of IF for up to 10 min, scale bar, 200 μm. (C-D) Representative fluorescence images of fluorescence recovery after photobleaching in collagen-containing microfluidic chips in the (C) presence or (D) absence of IF for up to 30 s, scale bar, 50 μm. (E) A rectangle ROI was used for quantifying the fluorescent signal of sodium fluorescein diffusion from the microfluidic chip in the presence or absence of IF. The mean fluorescence intensity of the ROI region was calculated using Image J at different time points. (F) A rectangle ROI was used for quantifying the fluorescent signal of fluorescence recovery after photobleaching from the microfluidic chip in the presence or absence of IF. The mean fluorescence intensity of the ROI region was calculated using Image J at different time points. (G-H) flow rate distribution simulations in the (G) presence or (H) absence of IF on microfluidic chip by COMSOL software.

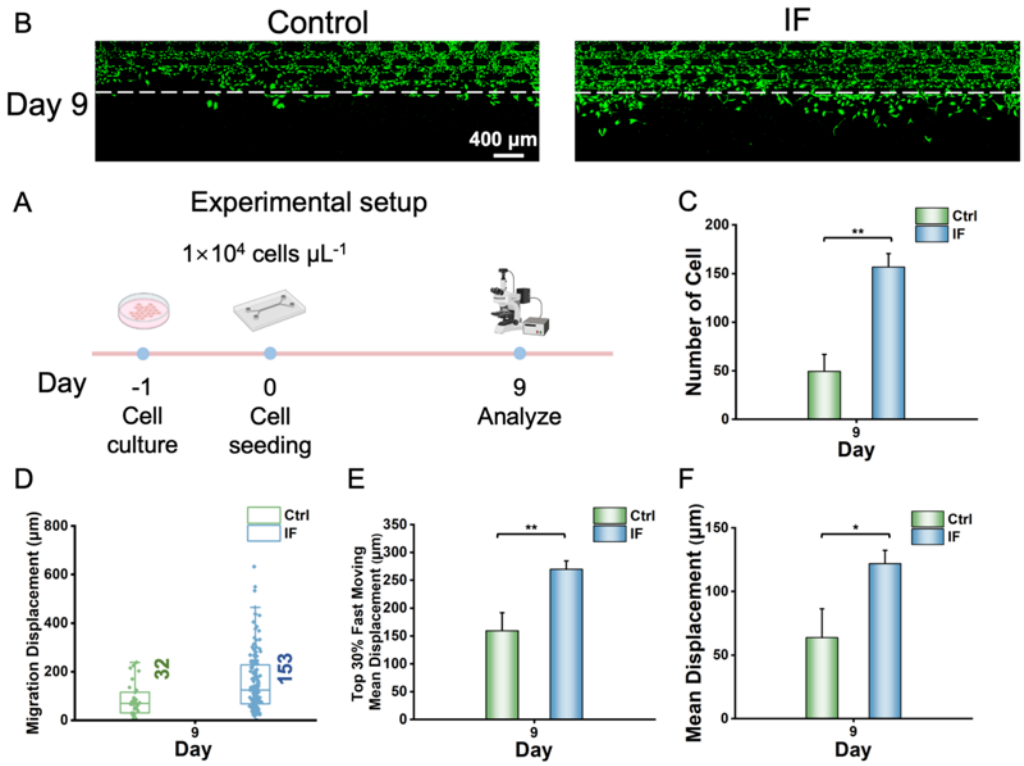


**Fig. S6** Migration analysis with low density U251 cells on microfluidic chip. A) Line diagram showing experimental plan. B) Representative fluorescence images of migrating cells on the microfluidic chips in control and IF conditions on day 9. Scale bars, 400 μm. C-F) Quantification of C) number of migrating cells, D) migration displacement on individual cell, E) the mean displacement of top 30% fast-moving migrating cells on each condition, F) and the mean displacement of migrating cells (n = 3 chips from 3 independent experiments).

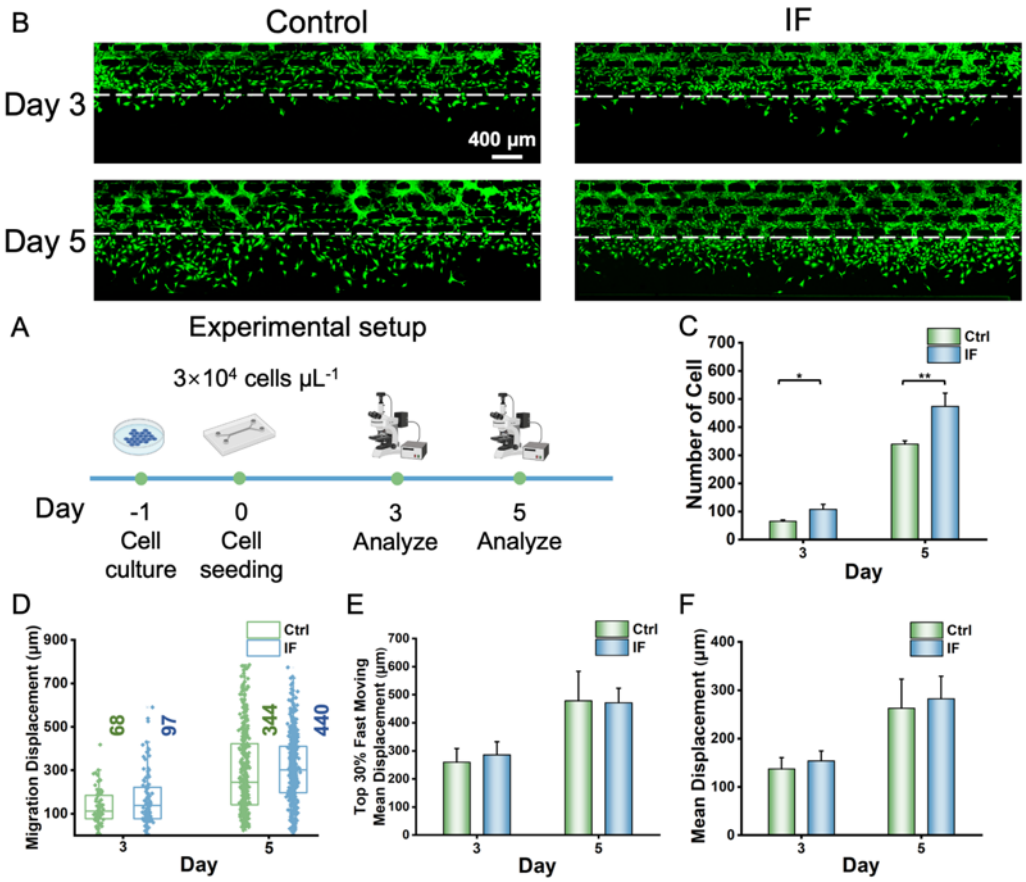


**Fig. S7** Migration analysis with high density U87-MG cells on microfluidic chip. A) Line diagram showing experimental plan. B) Representative fluorescence images of migrating cells on the microfluidic chips in control and IF conditions on day 3 and day 5. Scale bars, 400 μm. C-F) Quantification of C) number of migrating cells, D) migration displacement on individual cell, E) the mean displacement of top 30% fast-moving migrating cells on each condition, F) and the mean displacement of migrating cells (n = 3 chips from 3 independent experiments).

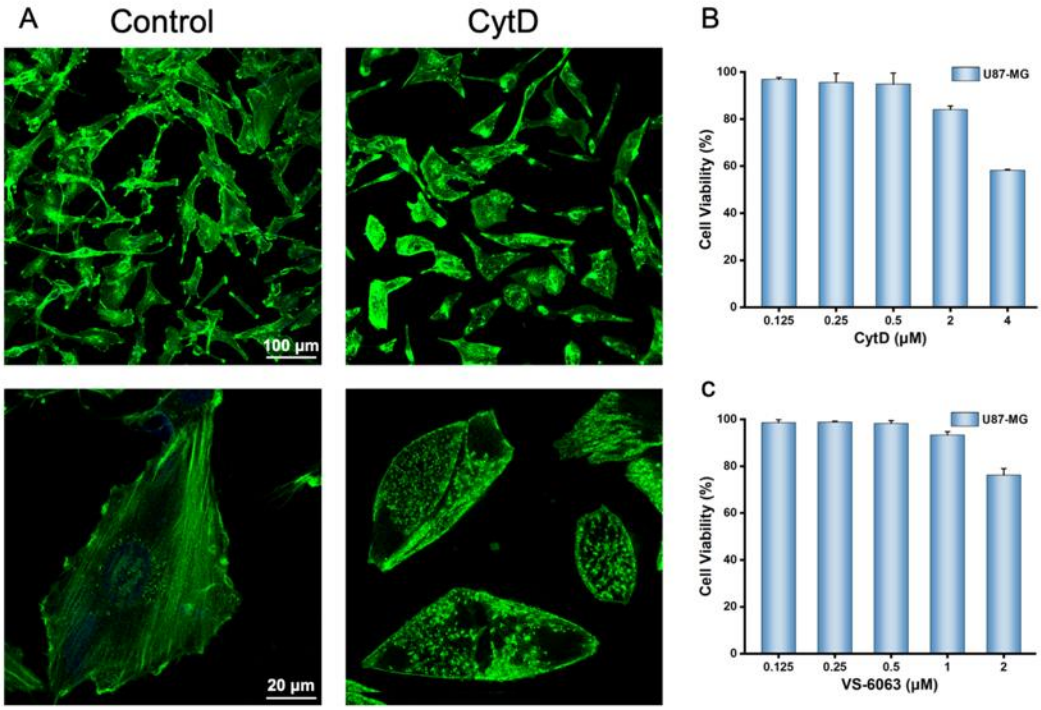


**Fig. S8** Characterization of cell cytoskeleton and toxicity of CytD and VS-6063. A) Representative fluorescence images of U87-MG cells stained with Actin-Tracker Green 488. Scale bars, 100 μm and 20 μm. B-C) Proliferation rates of U87-MG cells in different concentrations of B) CytD and C) VS-6063.

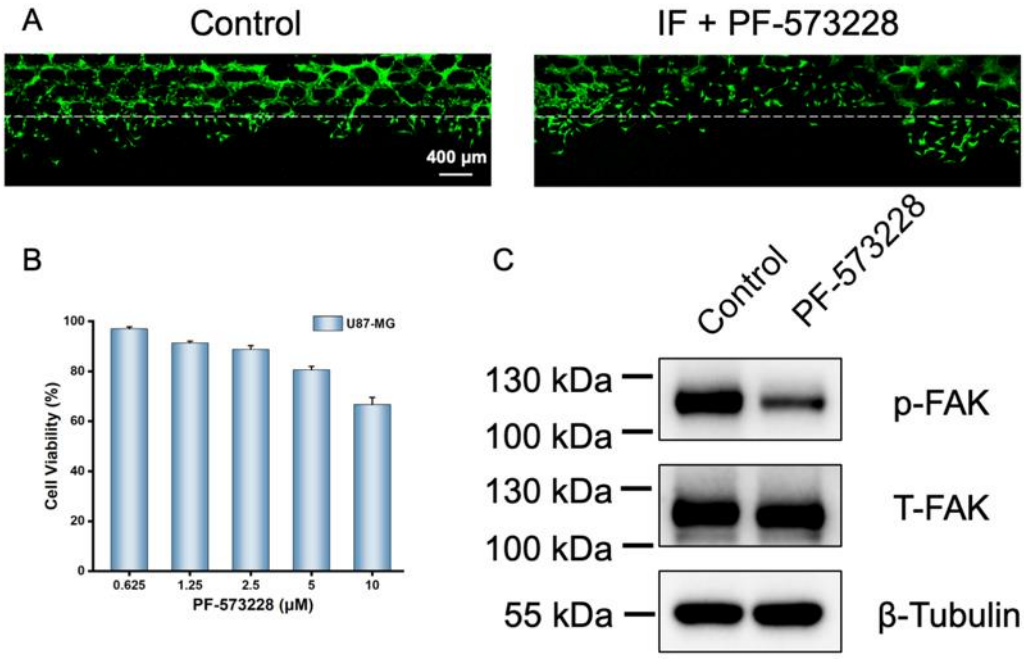


**Fig. S9** Migration analysis with U87-MG cells treated with PF-573228 on microfluidic chip. A) Representative fluorescence images of migrating cells on the microfluidic chips in control, and IF + 1.25 μM PF-573228 conditions on day 6. Scale bars, 400 μm. B) Proliferation rates of U87-MG cells in different concentrations of PF-573228. C) Western blot analysis of U87-MG cells treated with the PF-573228 at 1.25 μM for 48 h.

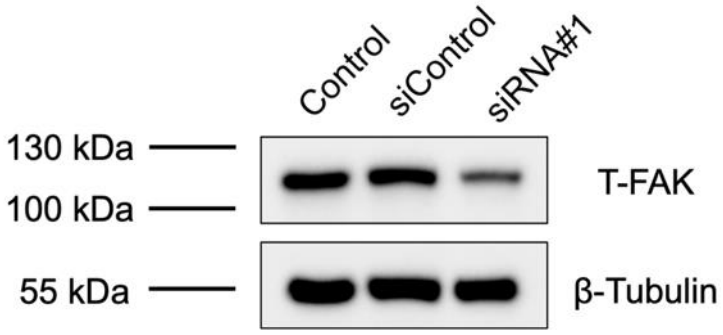


**Fig. S10** Western blot analysis of U87-MG cells treated with the siRNA#1 at 150 nM for 48 h.

**Table S1** Comparison of methods, flow rates, and research content of interstitial flows as described in the published literature

| Research article | Methods of realizing interstitial flow | Flow rate | Research contents | Ref |
|---|---|---|---|---|
| Construction of multilayered small intestine-like tissue by reproducing interstitial flow | syringe pumps | 30 μL $h^{-1}$ | A micro-small intestine system was successfully developed, incorporating interstitial flow and forming a multilayered structure, which can be beneficial for pharmaceutical and infectious disease research. | [1] |
| Interstitial flow potentiates TGF-β/Smad-signaling activity in lung cancer spheroids in a 3D-microfluidic chip | pressure pump | 0.1-1 μm $s^{-1}$ | A 3D matrix-based microfluidic platform was fabricated to investigate the potentiating effect of IF on exogenous TGF-β-induced Smad-signaling activity in A549 lung cancer spheroids. | [2] |

| Research article | Methods of realizing interstitial flow | Flow rate | Research contents | Ref |
|---|---|---|---|---|
| Convection and extracellular matrix binding control interstitial transport of extracellular vesicles | hydrostatic head pressure heads | 0.5-1 μm $s^{-1}$ | Finite element models reveal interstitial accumulation of high affinity binding EVs. | 3 |
| Extracellular Matrix-Derived Biophysical Cues Mediate Interstitial Flow-Induced Sprouting Angiogenesis | pipette tips | ~10.76 and 11.18 μm $s^{-1}$ | A 3D microfluidic biomimicry, featuring detailed characterization of hydrogel scaffolds, was fabricated to investigate how HA enhances interstitial flow-mediated angiogenic sprouting by altering the stiffness and pore size of the collagen ECM. | 4 |
| Multilayer microfluidic platform for the study of luminal, transmural, and interstitial flow | the connection of separate medium reservoirs | 0.15-0.30 μm $s^{-1}$ | A multi-layer microfluidic platform was fabricated that enables the culture of engineered blood and lymphatic microvessels, as well as the independent control of blood, lymphatic flow, and interstitial fluid pressures. | 5 |
| Interstitial flow enhances the formation, connectivity, and function of 3D brain microvascular networks generated within a microfluidic device | the connection of separate medium reservoirs | 0.005-10 μm $s^{-1}$ | Primary human brain endothelial cells, pericytes, and astrocytes were cultured within a 3D fibrin matrix, both with and without interstitial flow, on a microfluidic chip. | 6 |

| Research article | Methods of realizing interstitial flow | Flow rate | Research contents | Ref |
|---|---|---|---|---|
| A 3D human adipose tissue model within a microfluidic device | the connection of separate medium reservoirs and pipette tips | 0.17-1.08 μm $s^{-1}$ | A microfluidic system was presented that enables the on-chip differentiation of stem cells into a 3D adipose microtissue and subsequent analysis of adipocyte function under physiological interstitial flow conditions. | 7 |
| In vivo–mimicking microfluidic perfusion culture of pancreatic islet spheroids | osmotic pump | 1.54-5.05 μm $s^{-1}$ | Functional islet spheroids were fabricated using a microfluidic chip that incorporates interstitial flow. This dynamic culture enhances islet health and the maintenance of islet endothelial cells. | 8 |
| Microfluidic device to control interstitial flow-mediated homotypic and heterotypic cellular communication | pipette tips | 0-40 μm $s^{-1}$ | A novel microfluidic device has been developed, which can be utilized to investigate homotypic and heterotypic cell-cell communication patterns in biologically relevant 3D microenvironments. | 9 |
| Mechanotransduction of fluid stresses governs 3D cell migration | pipette tips | ~3 μm $s^{-1}$ | A microfluidic platform was fabricated to investigate the effects of interstitial fluid stresses imparted on cells embedded within a collagen type I hydrogel. | 10 |
| **This work** | **pipette tips** | **~6.57 μm $s^{-1}$** | **A microfluidic chip that mimics the cerebrospinal fluid circulation microenvironment is proposed to study the migration characteristics of glioblastoma cells in complex environments where glioblastoma coexists with diseases that elevate CSF levels.** | |

**Table S2** Comparison of the primary chemical constituents within extracellular solutions of DMEM, ACSF, and *in vivo* cerebrospinal fluid

| Components | DMEM | ACSF | CSF | Notes |
|---|---|---|---|---|
| Inorganic salts | + | + | + | $CaCl_2$, KCl, NaCl, $NaHCO_3$, $NaH_2PO_4$, $MgSO_4$, etc. |
| Amino Acids | + | - | -[a)] | L-Arg, L-Cys, L-Leu, L-Met, L-Glu, L-Val, etc. |
| Vitamins | + | - | - | D-Cal, Folic Acid, Riboflavin, etc. |
| Cytokines and signaling proteins | - | - | +[b)] | TNF-α, IL-6, ADA, LDH, LA, etc. |
| Other | + | - | -[a)] | Phenol red, Sodium pyruvate, HEPES, etc. |

Table Footnote: [a)] The asterisk denotes that only trace amounts of amino acids and vitamins are found *in vivo* within CSF.

[b)] The asterisk denotes that only trace amounts of cytokines and signaling proteins are found *in vivo* within CSF in healthy individuals.

**Table S3** siRNA sequence targeting FAK and negative control siRNA sequence

| Name | Sense Sequence | Antisense sequence |
|---|---|---|
| siRNA#1 | 5’-GAGAAUCCUGUCUGGAUAAUU-3’ | 5’-UUAUCCAGACAGGAUUCUCUG-3’ |
| siRNA#2 | 5’-CCGAUUGGAAACCAACAUAUU-3’ | 5’-UAUGUUGGUUUCCAAUCGGAC-3’ |
| Negative control | 5’-ACGCCUACGAUUCUUGUGAAA-3’ | 5’-UCACAAGAAUCGUAGGCGUCG-3’ |

**Table S4** Comparison of on-chip model, CSF simulation, geometrical simulation, IF rate simulation, human brain choroid plexus simulation, and research content as described in the published literature

| Research article | On-chip model | CSF simulation | Geometrical simulation | IF rate simulation | human brain choroid plexus simulation | Research content | Ref |
|---|---|---|---|---|---|---|---|
| New Neurons Follow the Flow of Cerebrospinal Fluid in the Adult Brain | No | No | No | No | No | neuroblast migration parallels CSF flow. | 11 |
| Human Cerebrospinal Fluid Modulates Pathways Promoting Glioblastoma Malignancy | No | No | No | No | No | CSF is a key player in determining tumor growth and invasion through the activation of complex gene expression patterns characteristic of a malignant phenotype. | 12 |
| Cerebrospinal fluid replacement solutions promote neuroglia migratory behaviors and spinal explant outgrowth in microfluidic culture | Yes | Yes | No | No | No | ShC responded chemotactically to BDNF stimuli generated within DMEM or EBS solutions with high similarity. | 13 |
| Engineering choroid plexus-on-a-chip with oscillatory flow for modeling brain metastasis | Yes | No | No | Yes | Yes | A reconstituted human brain choroid plexux on microfluidic chip under in vivo-like CSF flow exhibited a physiologically | 14 |

| Research article | On-chip model | CSF simulation | Geometrical simulation | IF rate simulation | human brain choroid plexus simulation | Research content | Ref |
|---|---|---|---|---|---|---|---|
| Heterogeneous Glioma Cell Invasion Under Interstitial Flow Depending on Their Differentiation Status | Yes | No | No | Yes | No | relevant tumor-immune microenvironment. The invasion and protrusion formation of glioma initiating cells (GICs) were significantly enhanced by forward interstitial flow in differentiated cell conditions. | 15 |
| **This work** | **Yes** | **Yes** | **Yes** | **Yes** | **No** | **A microfluidic chip that mimics the CSF circulation microenvironment is fabricated to study the migration characteristics of glioblastoma cells in complex environments where glioblastoma coexists with diseases that elevate CSF levels.** | |

**Movie S1** Representative movies of migration dynamics analysis using U87-MG cells in the control group.

**Movie S2** Representative movies of migration dynamics analysis using U87-MG cells in the IF group.

## References


1. S. Deguchi, K. Kosugi, N. Takeishi, Y. Watanabe, S. Morimoto, R. Negoro, F. Yokoi, H. Futatsusako, M. Nakajima-Koyama, M. Iwasaki, T. Yamamoto, Y. Kawaguchi, Y. S. Torisawa and K. Takayama, *Cell Stem Cell*, 2024, **31,** 1315-1326 e1318.
2. Z. Rahman, A. D. Bordoloi, H. Rouhana, M. Tavasso, G. van der Zon, V. Garbin, P. Ten Dijke and P. E. Boukany, *Lab Chip*, 2024, **24,** 422-433.
3. P. A. Sariano, R. R. Mizenko, V. S. Shirure, A. K. Brandt, B. B. Nguyen, C. Nesiri, B. S. Shergill, T. Brostoff, D. M. Rocke, A. D. Borowsky, R. P. Carney and S. C. George, *J. Extracell Vesicles*, 2023, **12,** e12323.
4. C. W. Chang, H. C. Shih, M. G. Cortes-Medina, P. E. Beshay, A. Avendano, A. J. Seibel, W. H. Liao, Y. C. Tung and J. W. Song, *ACS Appl. Mater. Interfaces*, 2023, **15,** 15047-15058.
5. G. H. Lee, S. A. Huang, W. Y. Aw, M. L. Rathod, C. Cho, F. S. Ligler and W. J. Polacheck, *Biofabrication*, 2022, **14,** 025007.
6. M. A. Winkelman, D. Y. Kim, S. Kakarla, A. Grath, N. Silvia and G. Dai, *Lab Chip*, 2021, **22,** 170-192.
7. F. Yang, A. Carmona, K. Stojkova, E. I. Garcia Huitron, A. Goddi, A. Bhushan, R. N. Cohen and E. M. Brey, *Lab Chip*, 2021, **21,** 435-446.
8. Y. Jun, J. Lee, S. Choi, J. H. Yang, M. Sander, S. Chung and S. H. Lee, *Sci. Adv.*, 2019, **5,** eaax4520.
9. L. F. Alonzo, M. L. Moya, V. S. Shirure and S. C. George, *Lab Chip*, 2015, **15,** 3521-3529.
10. W. J. Polacheck, A. E. German, A. Mammoto, D. E. Ingber and R. D. Kamm, *Proc. Natl. Acad. Sci. U S A*, 2014, **111,** 2447-2452.
11. K. Sawamoto, H. Wichterle, O. Gonzalez-Perez, J. A. Cholfin, M. Yamada, N. Spassky, N. S. Murcia, J. M. Garcia-Verdugo, O. Marin, J. L. Rubenstein, M. Tessier-Lavigne, H. Okano and A. Alvarez-Buylla, *Science*, 2006, **311,** 629-632.
12. A. Carrano, N. Zarco, J. Phillipps, M. Lara-Velazquez, P. Suarez-Meade, E. S. Norton, K. L. Chaichana, A. Quinones-Hinojosa, Y. W. Asmann and H. Guerrero-Cazares, *Front. Oncol.*, 2021, **11,** 624145.
13. R. N. Cliver, B. Ayers, A. Brady, B. L. Firestein and M. Vazquez, *J. Tissue. Eng. Regen. Med.*, 2021, **15,** 176-188.
14. J. Lim, S. Rhee, H. Choi, J. Lee, S. Kuttappan, T. T. Yves Nguyen, S. Choi, Y. Kim and N. L. Jeon, *Mater. Today Bio.*, 2023, **22,** 100773.

15. N. Namba, Y. Chonan, T. Nunokawa, O. Sampetrean, H. Saya and R. Sudo, *Tissue Eng. Part A*, 2021, **27,** 467-478.